Available online at www.sciencedirect.com
ScienceDirect
Applied Mathematics and Computation 185 (2007) 823–833
APPLIED MATHEMATICS AND COMPUTATION
www.elsevier.com/locate/amc

Enhanced gradient-based algorithm for the estimation of fingerprint orientation fields ☆

Yi Wang *, Jiankun Hu, Fengling Han

School of Computer Science and Information Technology, Royal Melbourne Institute of Technology, Melbourne VIC 3001, Australia

Abstract

An accurate estimation of fingerprint orientation fields is an essential step in the overall fingerprint recognition process. Conventional gradient-based approaches are popular but very sensitive to noise. In this paper, we propose a novel implementation to improve the performance of gradient-based methods. The enhanced algorithm chooses the best orientation estimate from four overlapping neighborhoods of every image block, where the voting scheme is based on the reliability measures. We test our algorithm on real fingerprint images. The experiment results suggest that our enhanced algorithm achieves visibly better noise resistance with modest computation time in comparison with other gradient-based methods.

Keywords: Automatic fingerprint recognition; Orientation estimation; Gradient-based algorithm; Biometric authentication

1. Introduction

With the pervasive growth of Internet computing, it is highly desired to have reliable safeguard for sensitive data and personal resources. Critical information of data transaction over the web can be encrypted using advanced cryptography methods [1] and data hiding techniques [2]. However, all these security measures are not capable of assuring the genuine users who indeed lodge the transaction requests. This vulnerability has been evidenced by numerous spoofing and intrusion attacks. Thus people are now more conscious than ever that the password based authentication is not secure enough.

Fingerprints are permanent physiological features of human beings. It is well established in science that they are highly distinctive between individuals [3]. This has provided the theoretical basis to use fingerprints as a reliable means for personal identification. In fact, fingerprint has been used in forensic science over a century. In the early days, identifying fingerprints is conducted manually. The tedious work is expensive and time consuming. Therefore, automatic fingerprint authentication has become a popular research topic over the last decades.

☆ This work is financially supported by the ARC Linkage Project LP0455324.
* Corresponding author.
E-mail addresses: alice@cs.rmit.edu.au (Y. Wang), jiankun@cs.rmit.edu.au (J. Hu), fengling@cs.rmit.edu.au (F. Han).

0096-3003/$ - see front matter
doi:10.1016/j.amc.2006.06.082

Fingerprint is constructed by ridges and valleys. The local ridge structures are commonly used to match two fingerprints topologically. The most prominent local ridge structures are ridge endings and bifurcations. Ridge endings refer to the terminals of ridge lines and ridge bifurcations are the fork-like structures. They are more often called minutiae in fingerprints. Since the locations and directions of minutiae are unique for every finger on every person [4], they form the base of fingerprint matching. The global features such as singularities also help to discriminate fingerprints. Singularities are special regions of fingerprints where the ridges assemble in discontinuous behavior. The process that extract these discriminative features from a fingerprint image and representing them in quantitative forms is called fingerprint recognition. Fig. 1 displays a simplified flowchart for such systems. As indicated in Jain et al. [5], a typical fingerprint recognition system consists of three main components: (1) orientation field estimation; (2) ridge enhancement and tinning; (3) minutiae extraction.

As shown in Fig. 1, orientation field estimation is an essential module of fingerprint recognition systems. The angles of orientation fields represent the ridge flow directions on regularly spaced grids. They help to reveal the intrinsic features of ridge topologies, and thus have critical impact on almost all subsequent processes [6]. For instance, it provides flow directions of ridges for directional filtering in ridge enhancement [7] and can detect the singularities [8]. Other uses of orientation field estimates are reported in the literature [9–11].

To obtain reliable ridge orientations, the most popular approach is to go through the gradients of gray intensity. There are some other methods proposed in the literature including filter-bank based approach [11], waveform projection [12] and spectral estimation [13]. However, it is reported that these methods do not provide as much accurate results as the gradient-based methods. This is mainly because most of them rely on a number of fixed possible templates or filters [3]. Some of these methods are also argued to be computational expensive as they involve exhaustive comparison process [14].

The gradient-based methods also have their limitations. Since the gradients of image intensity are usually computed on pixel level, the related methods are quite sensitive to noise even after the averaging/smoothing process. Mathematic modeling using Bayesian networks [6], complex polynomials [14] and rational polynomials [15] are introduced to manipulate the coarse orientation estimates. However, these model based approaches need to know the locations and types of singularities in a ridge pattern in order to adjust the system parameters. In such cases, the coarse orientation estimates are used to feed the training model as initial statistics. Therefore, it is still critical to have a good estimation of coarse orientation fields in the first place. A more accurate estimation of coarse orientation fields can also reduce the computation burden placed on the post processing stage. This is especially desired in the resource limited applications such as mobile devices and smart cards.

In this paper, we propose an enhanced gradient-based algorithm for coarse estimation of fingerprint orientation fields. The basic idea of our scheme is to estimate the dominant orientation of a base block from its four overlapping neighborhoods. The best estimate is then selected from the least noise-affected neighborhood according to some reliability measures. Our experiment results show that the enhanced algorithm achieves visibly better noise resistance with modest computation efficiency in comparison to other gradient-based methods.

The rest of the paper is organized as follows. Section 2 elaborates the technical background of general gradient-based approaches and related work. Section 3 presents our enhanced algorithm with noise analysis. Experiment results are demonstrated and evaluated in Section 4. Finally, we conclude in Section 5.

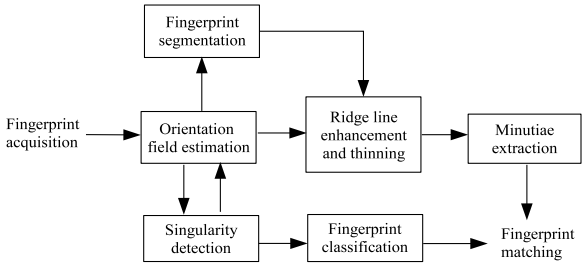

Fig. 1. Flowchart of typical fingerprint recognition systems.

2. Gradient-based methods

In the gradient-based methods, gradient vectors are first calculated by taking the partial derivatives of image intensity at each pixel in Cartesian coordinates. The gradient vectors can be denoted as $[g_x, g_y]^{\mathrm{T}}$. In a fingerprint image, the gradient vectors point to the highest variation of gray intensity which is perpendicular to the edge of ridge lines.

A fingerprint field orientation map is defined as a collection of two-dimensional direction fields. They represent the directions of ridge flows in regular spaced grids. The magnitudes of these fields can be omitted and only the angle information is of interest. An orientation map is commonly represented in the form of a matrix $\{\theta_{xy}\}$, where $\theta_{xy} \in [0, \pi]$. The orientation θ is orthogonal to $\bar{\varphi}$, where $\bar{\varphi}$ is the dominant gradient angle of a local base block.

Since a ridge line has two edges, the gradient vectors at both sides of a ridge are opposite to each other. If we want to calculate $\bar{\varphi}$ by taking the average of gradient angles directly in a local base block, the opposite gradients at both sides of a ridge line are likely to cancel each other. To solve this problem, Kass and Witkin [16] proposes a simple and clever idea of doubling the gradient angles before the averaging process so that $(\varphi + \pi)$ becomes $(2\varphi + 2\pi)$ which is equal to 2φ. In practice, 2φ are the angles of squared gradient vectors $[g_{sx}, g_{sy}]^{\mathrm{T}}$ that has the following relation with $[g_x, g_y]^{\mathrm{T}}$ according to trigonometric identities [8]:

$$\begin{bmatrix} g_{sx} \\ g_{sy} \end{bmatrix} = \begin{bmatrix} g^2 \cos 2\varphi \\ g^2 \sin 2\varphi \end{bmatrix} = \begin{bmatrix} g^2(\cos^2\varphi - \sin^2\varphi) \\ g^2(2\sin\varphi\cos\varphi) \end{bmatrix} = \begin{bmatrix} g_x^2 - g_y^2 \\ 2g_x g_y \end{bmatrix}. \tag{1}$$

The average squared gradient $[\bar{g}_{sx}, \bar{g}_{sy}]$ in a block specified by a window size W can be therefore calculated by

$$\begin{bmatrix} \bar{g}_{sx} \\ \bar{g}_{sy} \end{bmatrix} = \begin{bmatrix} \sum_W g_{sx} \\ \sum_W g_{sy} \end{bmatrix} = \begin{bmatrix} \sum_W (g_x^2 - g_y^2) \\ \sum_W 2g_x g_y \end{bmatrix}. \tag{2}$$

Conventional gradient-based methods divide the input fingerprint image into equal-sized blocks of $N \times N$ pixels, and average over each block independently. The direction of orientation field in a block B can be calculated by [8]

$$\theta_B = \frac{1}{2}\operatorname{atan}\left(\frac{\sum_{i=1}^{N}\sum_{j=1}^{N} 2g_x(i,j)g_y(i,j)}{\sum_{i=1}^{N}\sum_{j=1}^{N} g_x^2(i,j) - g_y^2(i,j)}\right) + \frac{\pi}{2}. \tag{3}$$

Note that function $\operatorname{atan}(\cdot)$ gives an angle value ranges in $[-\pi, \pi)$ which corresponds to the squared gradients, while θ_B is the desired orientation angle within $[0, \pi)$.

In order to measure the reliability of estimation for θ's, Kass and Witkin [16] introduces a metric called *coherence* that calculates the strength of the averaged gradient in the distribution of local gradient vectors. The coherence of a block B can be evaluated from [16]

$$\mathrm{Coh}_B = \frac{\left|\sum_{i=1}^{N}\sum_{j=1}^{N}(g_{sx}(i,j), g_{sy}(i,j))\right|}{\sum_{i=1}^{N}\sum_{i=1}^{N}|g_{sx}(i,j), g_{sy}(i,j)|}. \tag{4}$$

Instead of using equal-sized blocks, Jain et al. [17] proposes a hierarchical scheme to adjust the estimation resolution of local orientation fields via iterative steps. They introduce the concept of consistency level, which is a normalized deviation that compares the orientation estimates of the other blocks in a neighborhood from the centered objective block. If the consistency level is above a certain threshold, the local orientations around the objective block are re-estimated with a smaller window size.

3. New enhanced algorithm

In this section, we propose a new gradient-based algorithm that uses overlapping windows and a voting scheme. Because of the general parallel and anisotropy features, ridge patterns from the four overlapping

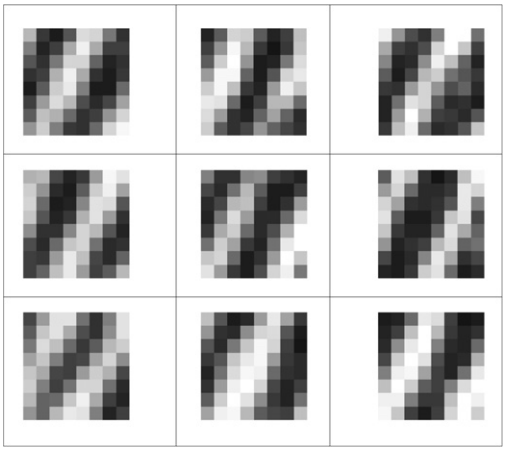

Fig. 2. A real fingerprint example site of 3×3 image blocks: paralleled ridge pattern.

neighborhoods of the target block are highly correlated to each other. If the window size is *small*, the ridge lines over the whole site are paralleled and slowly varied. A typical example of paralleled ridge pattern is shown in Fig. 2.

The proposed approach exploits the above salient feature of fingerprint ridge parallelism, thus enhance the traditional gradient-based methods. The algorithm is presented as follows. We first group every 2×2 adjoining blocks into a neighborhood D and every 3×3 adjoining blocks into a site with the four neighborhoods overlapping with each other. An example of such an organization is illustrated in Fig. 3.

Consider the centered block V in Fig. 3 for which the dominant orientation field is to be estimated. Let blocks $\{\mathrm{I}, \mathrm{II}, \mathrm{IV}, \mathrm{V}\}$ form a neighborhood marked D_1. Similarly, blocks $\{\mathrm{II}, \mathrm{III}, \mathrm{V}, \mathrm{VI}\}$ form D_2, blocks $\{\mathrm{IV}, \mathrm{V}, \mathrm{VII}, \mathrm{VIII}\}$ form D_3, and blocks $\{\mathrm{V}, \mathrm{VI}, \mathrm{VIII}, \mathrm{IX}\}$ form D_4. Note that the target block V is included in all four neighborhoods but positioned at different corners. From Eqs. (3) and (4), the averaged square gradients and the corresponding coherence measure can be calculated for each neighborhood D_a, D_b, D_c, D_d, respectively. The results yield two paired vectors $\theta = \{\theta_a, \theta_b, \theta_c, \theta_d\}$ and $\mathrm{Coh} = \{\mathrm{Coh}_a, \mathrm{Coh}_b, \mathrm{Coh}_c, \mathrm{Coh}_d\}$. We then find the maximum element in Coh and assign the corresponding angle in θ to the centered block 5. For instance, if

$$\mathrm{Coh}_b = \max\{\mathrm{Coh}_a, \mathrm{Coh}_b, \mathrm{Coh}_c, \mathrm{Coh}_d\},$$

then

$$\theta_5 = \theta_b.$$

To explain why this scheme can improve noise resistance of the estimation, let us first analyze the noise effect on a fingerprint image and the noise filtering using averaging process.

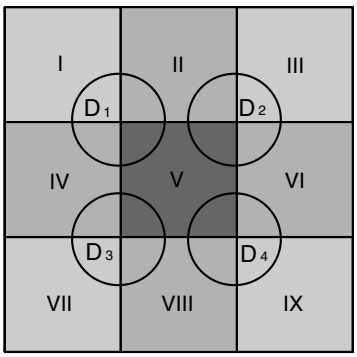

Fig. 3. A site consists of 3×3 blocks with the target block V in the center and four overlapping neighborhoods D_1, D_2, D_3, D_4.

One common type of noise appearing in fingerprint images is the smudges that link parallel ridges together. Smudges are usually caused by dirt and result in poor separation of ridge lines. We can make an assumption that the presence of dirt is uncorrelated and the random noise follows symmetric distribution with zero mean.

The ridge lines, on the contrary, have strong directions. That is, the variation of gray intensities along a ridge flow is much slower than that in its perpendicular direction. This feature is termed anisotropy [16]. In a smudged area, the anisotropy feature of ridge structures is corrupted by the random noise whose orientation pattern is symmetric distributed over all directions. Therefore, the resulting orientation estimate of the contaminated area is distracted.

Consider a noisy region composed of W pixels. The gradient vector at each pixel is composed of the true gradients of original ridges $[g_{tx}, g_{ty}]^T$ and the disturbance gradients of noise factor $[\Delta g_x, \Delta g_y]^T$. That is,

$$\begin{bmatrix} g_x \\ g_y \end{bmatrix} = \begin{bmatrix} g_{tx} + \Delta g_x \\ g_{ty} + \Delta g_y \end{bmatrix}. \tag{5}$$

Substituting Eq. (5) into Eq. (2) yields

$$\begin{bmatrix} \bar{g}_{sx} \\ \bar{g}_{sy} \end{bmatrix} = \begin{bmatrix} \sum_W g_{sx} \\ \sum_W g_{sy} \end{bmatrix} = \begin{bmatrix} \sum_W \left((g_{tx} + \Delta g_x)^2 - (g_{ty} + \Delta g_y)^2 \right) \\ \sum_W 2(g_{tx} + \Delta g_x)(g_{ty} + \Delta g_y) \end{bmatrix}. \tag{6}$$

Evaluate the above expression for $\bar{g}_{sx}$

$$\begin{aligned} \bar{g}_{sx} &= \sum_W (g_{tx} + \Delta g_x)^2 - (g_{ty} + \Delta g_y)^2 \\ &= \sum_W (g_{tx}^2 - g_{ty}^2) + 2\left(\sum_W g_{tx} \Delta g_x - \sum_W g_{ty} \Delta g_y \right) + \left(\sum_W \Delta g_x^2 - \sum_W \Delta g_y^2 \right). \end{aligned} \tag{7}$$

Since the variances of random noise in x and y directions are the same, the third term in the above equation can be crossed out. Therefore, Eq. (7) can be simplified as

$$\bar{g}_{sx} = \sum_W (g_{tx}^2 - g_{ty}^2) + 2\left(\sum_W g_{tx} \Delta g_x - \sum_W g_{ty} \Delta g_y \right), \tag{8}$$

where the first term is the expected value for $\bar{g}_{sx}$, the second term is the difference between the covariances of noise and the two original gradients.

Similarly, we can evaluate the expression for $\bar{g}_{sy}$ and have

$$\bar{g}_{sy} = \sum_W 2(g_{tx} + \Delta g_x)(g_{ty} + \Delta g_y) = 2\sum_W g_{tx} g_{ty} + 2\left(\sum_W g_{tx} \Delta g_y + \sum_W g_{ty} \Delta g_x \right) + 2\sum_W \Delta g_x \Delta g_y. \tag{9}$$

Since the original gradients and the noise gradients on the orthogonal directions are independent variables, the covariances in the second term above are equal to

$$\sum_W g_{tx} \Delta g_y = \sum_W g_{tx} \cdot \sum_W \Delta g_y = 0,$$
$$\sum_W g_{ty} \Delta g_x = \sum_W g_{ty} \cdot \sum_W \Delta g_x = 0,$$

noting that the mean of the noise distribution is zero.

Therefore, Eq. (9) can be simplified as

$$\bar{g}_{sy} = 2\sum_W g_{tx} g_{ty} + 2\sum_W \Delta g_x \Delta g_y. \tag{10}$$

If the noise factor is small (i.e., $\Delta g_y \to 0, \Delta g_x \to 0$), the last terms in both Eqs. (8) and (10) approach to zero, thus the estimation will be closer to the expected value. However, if the previous assumption of noise

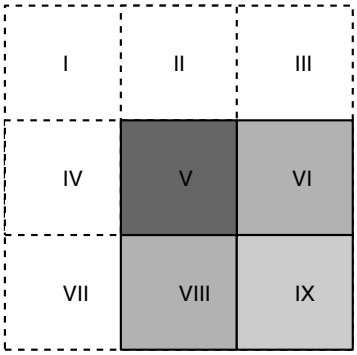

Fig. 4. A patched site where the target block is at an edge.

distribution is no longer symmetric with zero mean, the cross terms in Eqs. (7) and (9) cannot be canceled. For such cases, the estimates obtained from averaging over the same area can suffer from strong noise effects.

Since fingerprints can be viewed as smooth and continuous textures, ridge flows that pass through a base block are most likely to extend into one of the four neighborhoods that we defined previously. In our enhanced algorithm, we estimate $\bar{g}_{sx}$ and $\bar{g}_{sy}$ of each base block over four times rather than only once. Taking the example shown in Fig. 2, the four estimates would be $\bar{g}_{s(x,y)}|_{D_a}$, $\bar{g}_{s(x,y)}|_{D_b}$, $\bar{g}_{s(x,y)}|_{D_c}$ and $\bar{g}_{s(x,y)}|_{D_d}$. The best estimation is then selected from the least noise-affected neighborhood according to the reliability measure of coherence. Since the coherence measure in a region is influenced by the local noise effect, the redundant estimation from four different but overlapping neighborhoods is able to give better results.

Another interesting point is that our enhanced scheme actually separate the estimation window and the one that "watches" noise. That is, the averaging process is taken over each neighborhood while the noise is controlled in a bigger site that surrounds the centered objective block. As to eliminate noise, it is better to have larger window size to include more information of the ridge structures. But to maintain the resolution especially for high curvatures, a small estimation window is desired. In other gradient-based methods, the two are performed over the same window size which renders it more difficult to achieve the trade-off.

For a target block at an edge, we can apply the same algorithm by patching the site with virtual blocks of which the gradients are assumed to be zeros. An example of such scheme is illustrated in Fig. 4.

In the next section, we will present our experiment results to show the performance of our enhanced algorithm in comparison with the other gradient-based methods.

4. Experimental results and evaluation

We test our enhanced gradient-based method on real fingerprint images from FVC2000's sample databases [3]. All the tested fingerprint images are suffering from different noise effects caused by large creases, callus, moist or smudges. For the purpose of comparison, three gradient-based algorithms are evaluated on these fingerprint images: the conventional method [8,18], the hierarchical method [17] and our enhanced gradient-based method.

Since no ground truth exits for the evaluation of estimating fingerprint orientation fields, the measurement of objective error cannot be easily constructed [9,14]. Therefore, the noise resistance is often evaluated by manual observation for fingerprint orientation estimates. In the following section, we will display the compared orientation estimation results from the three gradient-based algorithms. The orientation fields are superimposed on the original gray scale fingerprint images. The results demonstrate that the proposed algorithm achieves superior estimation in comparison to the other two popular gradient-based methods.

Fig. 5a is a noisy segment of a fingerprint image. A sample site, which consists of 5×5 blocks, is snipped from the image and displayed in Fig. 5d. Fig. 5b prints the local orientation estimates using the conventional method introduced in Section 2. Fig. 5c depicts the coherence map where, the darker blocks represent higher coherence values closer to 1 and the brighter blocks represent lower coherence values closer to 0. Fig. 5e and f

provide the corresponding results obtained using our enhanced method, where we see that the orientation fields are more resilient to noise than those obtained from the conventional method in Fig. 5b.

Fig. 6a is a smudged segment cropped from a fingerprint image. The ridge pattern contains an indistinct left loop structure because the upper left corner is smeared by noise. To extract the orientation fields, we first

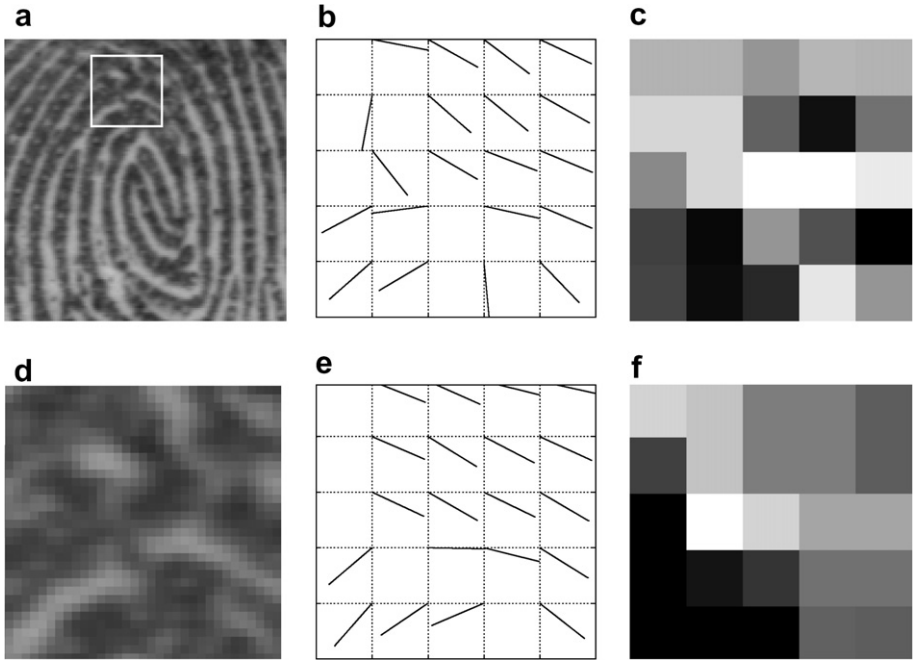

Fig. 5. (a) A segment of fingerprint image with the noisy sample area labeled in the white box; (b) the local field orientation map for the noisy sample area estimated from the conventional method; (c) the corresponding coherence map for (b); (d) the noisy sample area snipped from (a); (e) the local field orientation map estimated from our enhanced algorithm and (f) the corresponding coherence map for (e).

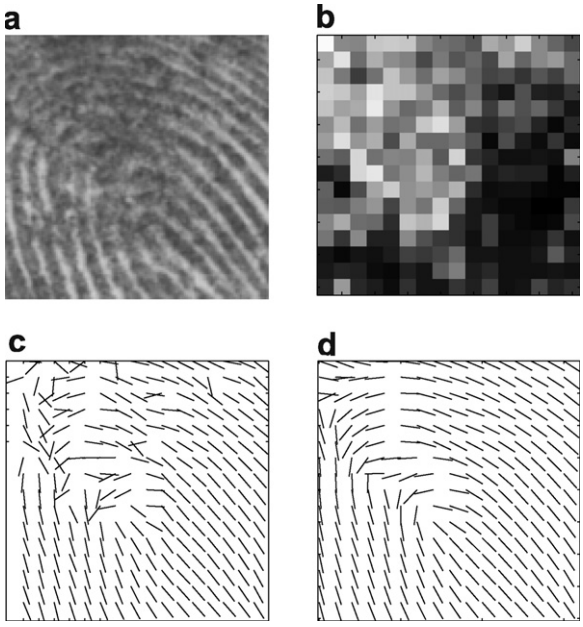

Fig. 6. (a) A loop type fingerprint segment with smudged areas on top left; (b) the coherence map; (c) orientation estimates produced by the conventional method and (d) orientation estimates produced by our enhanced method.

divide the segment into small grids. The associated coherence level of each grid is printed in Fig. 6b. We see the smudged areas (upper left) are brighter in Fig. 6b, which means the coherence values at those positions are lower. Fig. 6c is the estimation results from the conventional method, where the orientation fields are in a clutter at the top left. Fig. 6d shows a set of estimates using our weighted averaging method. One can see that the left loop structure is clearly revealed in Fig. 6d.

Because of the limited space, we can only demonstrate the estimation results of four complete fingerprint images in the following section. The examples are from four major fingerprint categories: twin loop, loop, arch and whorl. The size of each image is 256×364 pixels. The orientation estimates obtained from the three comparing algorithms are superimposed on the original gray scale fingerprint images respectively.

Fig. 7a shows a fingerprint with a big round callus at the upper right site. The bubble-like blotch can be seen as a strong noise factor. The orientation fields estimated from the conventional method is disturbed around the blotch area. The hierarchical scheme improves the estimation but it is still distracted at the bubble place. Among the three algorithms, only our enhanced algorithm can recover the ridge flow tendency smoothly at the edge of the blotch.

Fig. 7b displays a left loop type fingerprint. There are several vertical and horizontal creases running through the fingertip. This has caused some noise disturbance in the estimation results using both the conventional and the hierarchical methods. Comparatively, our enhanced method generates smoother estimates that align well with the original gray scale ridge flows as shown in the figure.

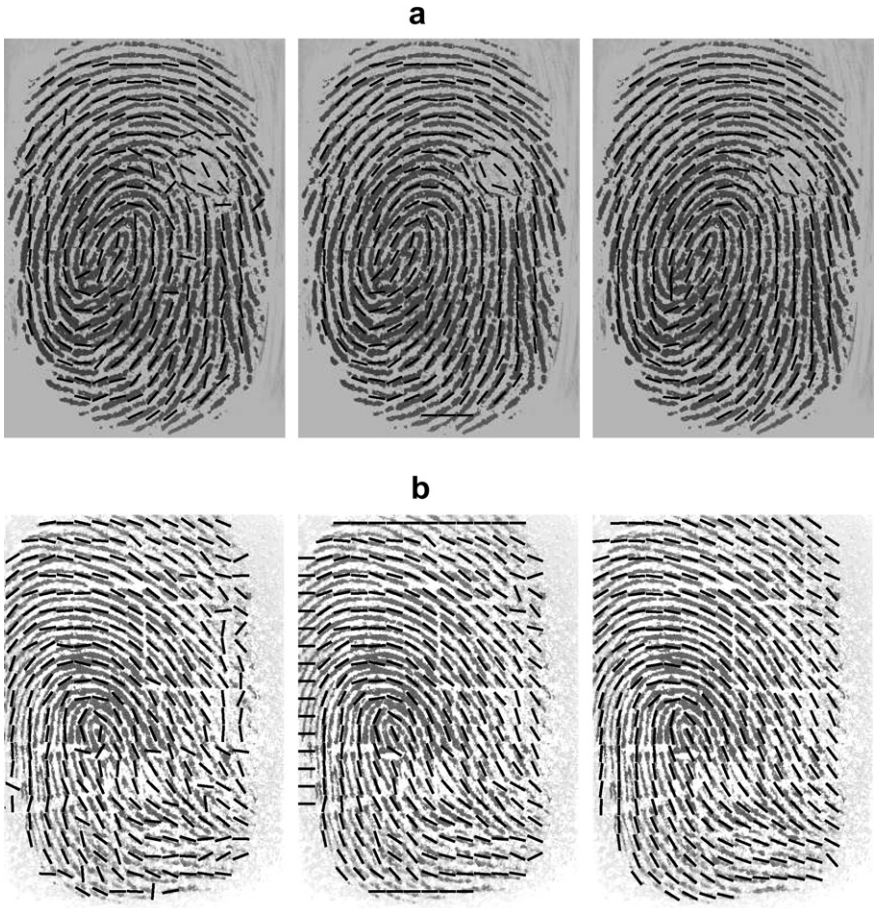

Fig. 7. Two sets of fingerprint examples. The column images from the left to the right are orientation results estimated from the conventional method, the hierarchical method and our enhanced gradient based method, respectively. (a) A twin loop type fingerprint with a bubble blotch and (b) a left loop type fingerprint with creases.

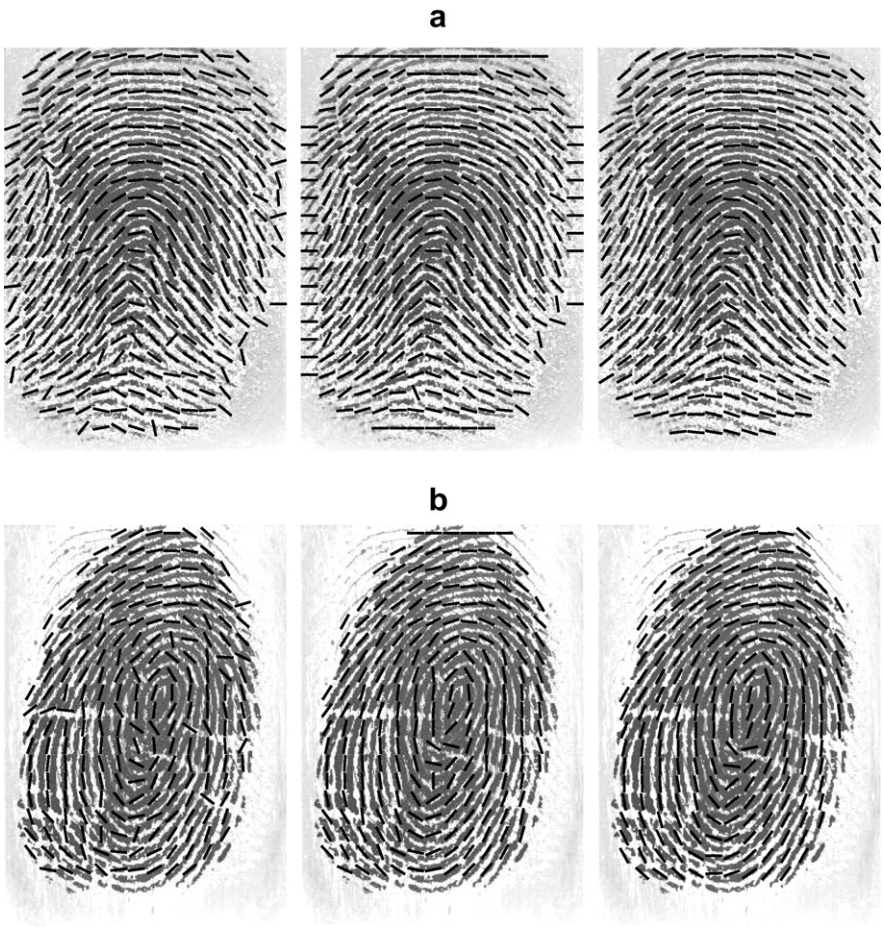

Fig. 8. Another two sets of fingerprint examples. The column images from the left to the right are orientation results estimated from the conventional method, the hierarchical method and our enhanced gradient based method, respectively. (a) An arch-type fingerprint with a scar and (b) a whorl type fingerprint with moist and creases.

Fig. 8 displays two other types of fingerprints in each row. The arch-type fingerprint in the first row has a remarkable scar at the top left. The whorl type fingerprint in the second row is affected by moist and creases. For these fingerprint examples, it is also visible in the figures that our enhanced method is more robust to the noise effects in comparison with the other two gradient-based methods.

We use the elapsed time of estimation to evaluate the computation efficiency for the three different gradient-based methods. The algorithms are implemented in MATLAB and the programs are run on a 2 GHz Pentium IV machine. The time records for the fingerprint examples displayed in Figs. 7a and 8 are tabulated in Table 1.

In general, the conventional method is the fastest among the three. The time used by our enhanced method with overlapping overheads is modest. The hierarchical scheme takes the longest computation time due to the

Table 1
Elapsed time of estimating the orientation fields using the conventional method, the hierarchical scheme and our enhanced algorithm

	Conventional method (s)	Enhanced method (s)	Hierarchical method (s)
Fig. 7a	0.467186	1.03215	1.575559
Fig. 7b	0.456284	1.459298	1.735545
Fig. 8a	0.451588	1.038511	1.358474
Fig. 8b	0.448014	0.966371	1.767948

Table 2
The average of the normalized elapsed time for all tested fingerprints

Conventional method	Enhanced method	Hierarchical method
1	2.35443	3.494963

iterative process it involves. We further normalize every triplet of the elapsed time with respect to that used by the conventional method. In other words, the normalization function can be expressed as

$$\text{Normalized time using the } X \text{ method} = \frac{\text{Elapsed time using the } X \text{ method}}{\text{Elapsed time using the conventional method}}. \tag{11}$$

We then take the average value of the normalized time of the triplets for all tested fingerprints and listed it in Table 2.

The conventional method has a standard normalized value of 1. From the results shown in Table 2, our enhanced gradient-based method is about 2.3 times slower than the conventional method, while the hierarchical method is about 3.5 times slower. Although our enhanced method is of modest speed among the three, it is worth to note that the enhanced method is capable in achieving visibly better noise resistance according to our sample experiments demonstrated in the first part of this session.

5. Conclusions

In this paper, a simple yet effective overlapping algorithm is proposed to improve the performance of gradient-based methods in coarse orientation field estimation of fingerprints. The enhanced algorithm chooses the best estimate from four overlapping neighborhoods based on their reliability measures. Unlike other gradient-based methods, our scheme conducts redundant estimations in a window size smaller than the one that controls noise. Therefore, it can achieve better trade-off between estimation resolution and noise filtering. Although the proposed algorithm includes an overlapping computation process, the overhead is only an averaging calculation. Hence the computation cost is less than those involving iterative steps. We test our algorithm on real fingerprint images from a public database. The experiment results show that our enhanced scheme yields visibly better orientation estimates for noisy fingerprint images with modest computation efficiency in comparison to other popular gradient-based methods used in the literature.

References

[1] W. Mao, Modern Cryptography: Theory and Practice, Prentice Hall PTR, Upper Saddle River, NJ, 2004.
[2] S. Katzenbeisser, F.A.P. Petitcolas, Information Hiding Techniques for Steganography and Digital Watermarking, Artech House, Boston, London, 2000.
[3] D. Maltoni, D. Maio, A.K. Jain, S. Prabhakar, Handbook of Fingerprint Recognition, Springer Verlag, New York, 2003.
[4] N.K. Ratha, R. Bolle, Automatic Fingerprint Recognition Systems, Springer Verlag, New York, 2004.
[5] A.K. Jain, L. Hong, S. Pankanti, R. Bolle, An identity-authentication system using fingerprints, Proc. IEEE 85 (1997) 1365–1388.
[6] S.C. Dass, Markov random field models for directional field and singularity extraction in fingerprint images, IEEE Trans. Image Process. 13 (2004) 1358–1367.
[7] A. Jain, S. Prabhakar, L. Hong, S. Pankanti, Filterbank-based fingerprint matching, IEEE Trans. Image Process. 9 (2000) 846–859.
[8] A.M. Bazen, S.H. Gerez, Systematic methods for the computation of the directional fields and singular points of fingerprints, IEEE Trans. Pattern Anal. Machine Intell. 24 (2002) 905–919.
[9] N. Ratha, S. Chen, A.K. Jain, Adaptive flow orientation based feature extraction in fingerprint images, Pattern Recogn. 28 (1995) 1657–1672.
[10] K. Karu, A.K. Jain, Fingerprint classification, Pattern Recogn. 17 (1996) 389404.
[11] A.K. Jain, S. Pankanti, L. Hong, A multichannel approach to fingerprint classification, IEEE Trans. Pattern Anal. Machine Intell. 21 (1999) 348–359.
[12] B.G. Sherlock, D.M. Monro, K. Millard, Fingerprint enhancement by directional Fourier filtering, IEE Proc. Vision, Image Signal Process. 141 (1994) 87–94.
[13] C.L. Wilson, G.T. Candela, C.I. Watson, Neural network fingerprint classification, J. Artif. Neural Networks 1 (1994) 203–228.
[14] J. Zhou, J. Gu, A model-based method for the computation of fingerprints' orientation field, IEEE Trans. Image Process. 13 (2004) 821–835.
[15] B. Sherlock, D. Monro, A model for interpreting fingerprint topology, Pattern Recogn. 26 (1993) 1047–1055.

[16] M. Kass, A. Witkin, Analyzing oriented patterns, Comput. Vision, Graph. Image Process. 37 (1987) 362–385.
[17] A.K. Jain, L. Hong, R. Bolle, On-line fingerprint verification, IEEE Trans. Pattern Anal. Machine Intell. 19 (1997) 302–314.
[18] A.R. Rao, R.C. Jain, Computerized flow field analysis: oriented texture fields, IEEE Trans. Pattern Anal. Machine Intell. 14 (1992) 693–709.